Proceedings of the ASME 2011 Dynamic Systems and Control Conference
DSCC2011
October 31 - November 2, 2011, Arlington, VA, USA

DSCC2011-6072

ANTI-WINDUP LPV CONTROL DESIGN OF MR DAMPERS FOR STRUCTURAL VIBRATION SUPPRESSION

Mona Meisami-Azad
Dept. of Mechanical Engineering
University of Houston
Houston, TX 77004
Email: mmeisami@mail.uh.edu

Farzad A. Shirazi
Dept. of Mechanical Engineering
University of Houston
Houston, TX 77004
Email: fashiraz@mail.uh.edu

Karolos M. Grigoriadis
Dept of Mechanical Engineering
University of Houston
Houston, TX 77004
Email: karolos@uh.edu

ABSTRACT

Magneto-rheological (MR) dampers that belong to the family of semi-active devices are widely used for vibration attenuation in space and civil engineering structures. In this paper, we study the use of MR dampers for seismic protection of a model two-story structure. A modified Bingham model of the MR damper is considered for linear parameter varying (LPV) modeling and control of the system. The main contribution of the paper is the design and experimental validation of an LPV anti-windup compensator to tackle the effect of actuator saturation on control design performance. The designed LPV anti-windup control scheme is advantageous from the implementation standpoint because it can be considered as an addition to the existing control system. Experimental results demonstrate the effective vibration suppression of the structure in the presence of the seismic excitation inputs by utilizing an LPV control strategy. An inner/outer loop control strategy is further developed and implemented considering the actuator saturation effect to reduce the control effort and saving the MR damper power consumption.

INTRODUCTION

Magneto-rheological (MR) dampers are semi-active devices utilizing MR fluids. The MR fluid has the ability to transform into a near solid material in milliseconds when exposed to a magnetic field. It can return to its original liquid state, equally fast upon the removal of the magnetic field. The effect can be seen as a very large change in its effective viscosity. This allows the damping characteristics to be continuously controlled by varying the voltage applied to the MR damper. This semi-active device has been shown to be promising in seismic vibration reduction in civil engineering structures due to its desirable mechanical properties [1]. MR dampers have been additionally applied in a number of other applications including aerospace systems [2] biomedical applications [3] and automotive suspension systems [4].

Various models in the literature have been proposed to capture the dynamics of MR dampers. The Bingham model is an idealized mechanical model based on the Bingham behavior. This model uses a Coulomb friction element in parallel with a viscous damper [1]. The Bouc-Wen model is another model used to account for hysteresis in MR damper modeling [5]. The LuGre model is a simpler model with fewer number of parameters and has been used effectively in combination with adaptive parameter estimation methods [6]. Black-box approaches have also been used in modeling and identification of MR dampers [7]. Additionally, neural network approach have been developed for both identification and control of MR dampers [8].

Different MR damper control strategies have been proposed in the past. One control scheme that has received a lot of attention is the so-called clipped optimal control [4, 9]. Erkus *et al*. [10] applied the clipped optimal control method for vibration reduction of elevated highway bridges, where they compared performance of the LQR-clipped optimal controller with that of passive and active LQR controllers. Jansen and Dyke [9] carried out a comparative study between various control methods for MR damper control, including a Lyapunov-based controller, a decentralized bang-bang controller, maximum energy dissipation, a

clipped-optimal controller and modulated homogenous friction. The controllers were tested for vibration reduction of a six-story building exposed to large earthquake excitations. Poussot-Vassal *et al*. [11] designed and implemented a controller in the linear parameter varying (LPV) framework for semi-actively controlled devices. It is noted that the gain-scheduled control design method in [11] does not consider an LPV model that explicitly incorporates the MR damper properties. Du *et al*. [12] also developed and tested an $\mathcal{H}_\infty$ controller for MR-based vibration suppression in a quarter car model. Guo *et al*. [8] used a neuronetwork approach in a MR cable vibration suppression, where a neural network-based controller was designed to emulate LQG and clipped LQG controllers.

Anti-windup control design is employed to account for the cases, where the calculated controller output is different from the signal that is actually entering the plant. Actuator saturation is one of the main reasons why anti-windup compensation is used. In a linear control design, performance degradation, large overshoots and possible instability can be encountered if the actuator saturation is ignored during the linear control design process [13]. The goal of anti-windup compensation is to modify nominal controllers so that if the signal from the controller is different from that entering the plant, a corrective feedback action is taken to reduce the discrepancy. There are two schemes of anti-windup control where the first one takes the saturation nonlinearity into account from the beginning of the controller design and in the other one the linear controller is designed first followed by a modification to compensate for the saturation effects. As an example of the first scheme, Teel [14] proposed low-gain controllers using $\mathcal{H}_\infty$ optimal control theory. Nguyen and Jabbari [15] formulated an anti-windup control design problem for the amplitude and rate saturation nonlinearities in the form of a convex optimization problem through linear matrix inequalities (LMIs). Due to the combination of various requirements, this single-step approach may become conservative and quite complicated. An early review of the anti-windup control methods was reported in [16] and the anti-windup compensator synthesis problem was approached in an $\mathcal{H}_\infty$ framework in this paper.

In this paper, we design an LPV anti-windup compensator for a two-story building prototype using an MR damper for base isolation and vibration attenuation. It is experimentally validated that under some earthquake excitations the controllable voltage of MR damper exceeds the allowable upper and lower voltage limits resulting in performance degradation, as well as a high power consumption. However, with the use of an anti-windup compensator we are able to: (i) keep the MR damper voltage within an allowable range and hence maintain the power consumption in a low level, and (ii) maintain the closed-loop system performance. In our work, the LPV anti-windup controller designed to minimize the adverse effect of the saturation is integrated with a nominal controller. The synthesis condition for an anti-windup compensator design is formulated as a linear matrix inequality (LMI) optimization problem that can be solved efficiently.

EXPERIMENTAL SETUP

The experimental setup used in this work is shown in Figure 1. It consists of the following main parts: the shaking table and its driving components, a two-story model building, the MR damper, and sensors for displacement and acceleration measurements. The base-isolated two-story model building is supported by a slider with low friction providing the base isolation. The base mass consists of the slider mass and a $205.7\times50.69\times6.51$ mm^3 aluminum plate. The mass of the first and second floors consist of the same aluminum plate and additional weights. The side plates are aluminum beams with dimensions of $17.60\times50.69\times0.75$ mm^3. Two springs with the total stiffness of 1057 N/m are symmetrically attached to the base mass to restrict the base drift. The shaking table used in this study is the Shaker II by Quanser company that can provide $\pm$7.5 cm maximum displacement, $\pm$83.8 cm/s peak velocity, and $\pm$24.5 m/s^2 peak acceleration with a 930 kg bearing load carrying. The operational bandwidth of the table is 0-20 Hz. Customized earthquake wave signals from real earthquakes can be simulated with the shaker.

The displacement of the base and first floors are measured by two LB-70 series laser displacement sensors by KEYENCE company. The measurement range is 100 mm $\pm$40 mm with fastest response time of 0.7 ms (with sensitivity of 180 μm) and a maximum sensitivity of 10 μm (at the response time of 500 ms). Accelerations of the second and the base floors are captured by MEMS accelerometers attached to each floor by wax. The type of accelerometer used is ADXL203EB Rev.0 by Analog Device company. The measurement range is $\pm1.7g$, and the sensitivity is 1 mg in 60 Hz satisfying the requirements of the experiment, where $g = 9.81$ m/s^2 is the standard gravity. The dSPACE board DS1103 RD, with controller and communication board CLP 1103, is used for the data acquisition purposes. This board is linked with Matlab/Simulink via A/D and D/A converters and controls input and output signals in real-time. Furthermore, an Agilent 6542A programmable power supply is connected to the dSPACE board output to amplify the voltage applied to the MR damper. The sampling rate is set to be 500 Hz.

The MR damper under study is a custom-made device built in the Smart Material and Structure Laboratory at the University of Houston. This device is a sponge-type damper that provides a stiction effect taken into account in parameter identification and controller design processes. The damper consists of a magnetic coil, MR fluid and a sliding bar. The coil is excited by the voltage applied to the MR damper which increases the viscosity of MR fluid and consequently the force exerted on the sliding bar. The amount of force produced is proportional to the area of active MR sponge exposed to the magnetic field. The MR damper is excited by voltages up to 8 volts. The MR damper is attached between the base and a fixed point on the table to reduce the vibration of the structure. The damper stroke is $\pm$2 cm and can approximately produce a maximum force of 10N at the voltage of 8V. The dynamic equations of motion for the structure including

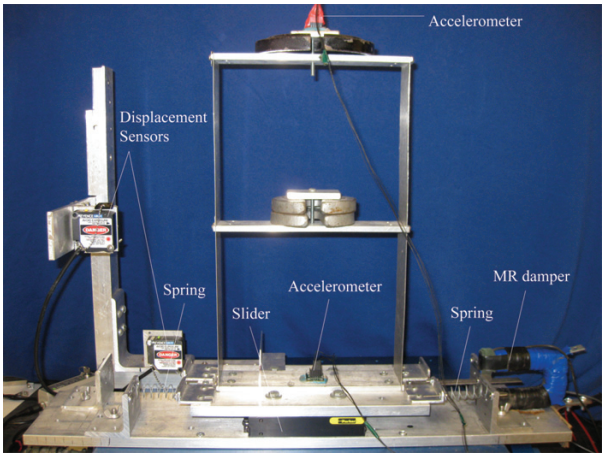

Figure 1. MR damper experimental test bed

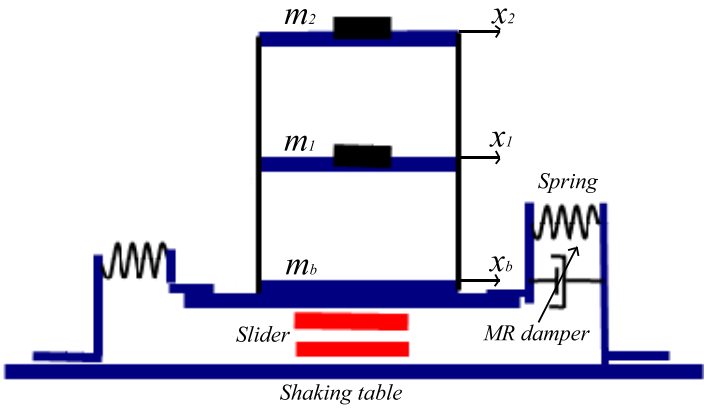

Figure 2. Schematic of the experimental setup

the MR damper (shown in Figure 2) is expressed as follows:

$$\mathcal{M}\ddot{q} + \mathcal{C}\dot{q} + \mathcal{K}q = \Gamma F_{mr} - \mathcal{M}\Lambda\ddot{x}_g \tag{1}$$

where $q = [x_b \;\; x_1 \;\; x_2]^T$, and $\Lambda = [1 \;\; 1 \;\; 1]^T$ and $\Gamma = [-1 \;\; 0 \;\; 0]^T$ are the distribution vectors. Here, x_b, x_1 and x_2 denote the displacement of the base, first floor and second floor, respectively. The excitation $\ddot{x}_g$ represents the ground acceleration.

The modal parameters of the structure have been experimentally identified. The identified mass, stiffness and damping matrices of the structure are as follows:

$$\mathcal{M} = \begin{bmatrix} 1.958 & 0 & 0 \\ 0 & 1.258 & 0 \\ 0 & 0 & 1.212 \end{bmatrix} [\mathrm{kg}],$$

$$\mathcal{C} = \begin{bmatrix} 1.281 & -0.487 & 0 \\ -0.487 & 1.325 & -0.599 \\ 0 & -0.599 & 0.829 \end{bmatrix} [\mathrm{N.s/m}],$$

$$\mathcal{K} = \begin{bmatrix} 2275.6 & -1218.6 & 0 \\ -1218.6 & 2716.3 & -1497.7 \\ 0 & -1497.7 & 1497.7 \end{bmatrix} [\mathrm{N/m}]$$

where the natural frequencies of the system are 2.1 Hz, 5.48 Hz and 9 Hz. Figure 2 shows the schematic of the experimental setup. The matrices above are represented based on $q = [x_b, x_1, x_2]^T$ as the displacement vector. The stiffness and damping coefficients corresponding to the base floor include the stiffness of the springs attached to the base and damping effect of the slider, respectively. A damping ratio of 1% has been assumed for all the structural modes. The proportional damping matrix has been obtained from $\mathcal{C} = a_0\mathcal{M} + a_1\mathcal{K}$, where a_0=0.1893 and a_1=0.0004.

The LuGre model representing MR damper dynamics is used for simulation purposes while the Bingham model is considered for control design due to its simple structure. All the experimentally identified parameters of both models are reported in [17].

LPV MODELING AND CONTROL DESIGN

Modified Bingham and LuGre-based models have been proposed to capture the dynamic behavior of an MR damper with stiction effect [17]. The parameters of the Bingham and LuGre models can be identified by solving a nonlinear optimization problem, and the identified models are validated experimentally for different operating conditions. In the present work, the MR damper is used to attenuate the vibration of a two-story model structure by designing an LPV controller where the base velocity is used as the scheduling parameter. The Bingham model, that has a simpler structure than other existing models, is employed to capture the nonlinear dynamics of the damper. Considering the stiction effect, the force produced by the MR damper is given by:

$$F_{mr} = (f_a + f_b V)\mathtt{sign}(\dot{x}_b) + (c_0\dot{x}_b + c_{0v}\dot{x}_b V)e^{-(\frac{\dot{x}_b}{v_0})^2} \tag{2}$$

where F_{mr} is the MR damper force when in motion (N), V is the input voltage (V), f_a is the Coulomb frictional force (N), f_b is the Coulomb frictional force influenced by voltage V (N/V), c_0 is the viscous damping coefficient (N.s/m), c_{0v} is the viscous damping coefficient influenced by voltage V (N.s/(m.V)), and v_0 is the normalizing velocity (m/s). This model is valid for non-zero velocities. The exponential term introduced in the model capture two effects: (i) the flattening effect expected at high velocities, and (ii) the stiction effect in low forces. The first effect is physically motivated by the change of the damping characteristics as the velocity increases due to more lubricant being forced into the interface. The second effect is more significant in low forces in which bumpy responses are observed in velocities close to zero. By assuming $\xi = [q \;\; \dot{q}]^T$, (1) can be rewritten in the state-space

form as follows:

$$\dot{\xi} = \begin{bmatrix} 0 & I \\ -\mathcal{M}^{-1}\mathcal{K} & -\mathcal{M}^{-1}\mathcal{C} \end{bmatrix} \xi + \begin{bmatrix} 0 \\ -\Lambda \end{bmatrix} \ddot{x}_g + \begin{bmatrix} 0 \\ \mathcal{M}^{-1}\Gamma \end{bmatrix} F_{mr} \tag{3}$$

where F_{mr} is the control input acting on the structure. It is, however, noted that the MR damper force cannot be directly controlled; instead the voltage is the control input.

It is desired to represent the nonlinear model obtained from combining (1) and (2) into an equivalent LPV form. To this purpose, we determine a quasi-LPV representation of the system model. Quasi-LPV (qLPV) systems represent a special class of LPV systems where the scheduling variables contain system states [18]. To proceed with the qLPV modeling of the system under study, we replace the MR damper force with the modified Bingham model in (2). Therefore, the equation of motion for the base mass is rewritten as follows:

$$m_b\ddot{x}_b + c_1(\dot{x}_b - \dot{x}_1) + c_b\dot{x}_b + c_0\dot{x}_b e^{-(\frac{\dot{x}_b}{v_0})^2} + k_1(x_b - x_1) + k_b x_b = -f_a \mathtt{sign}(\dot{x}_b) + (-f_b \mathtt{sign}(\dot{x}_b) - c_{0v}\dot{x}_b e^{-(\frac{\dot{x}_b}{v_0})^2})V - m_b\ddot{x}_g$$

Thus, we can rewrite (1) as follows considering the voltage as the input instead of the damper force:

$$\mathcal{M}\ddot{q} + \mathcal{C}_m\dot{q} + \mathcal{K}q = \Gamma_m V - \mathcal{M}\Lambda\ddot{x}_g \tag{4}$$

where the modified matrices C_m and Γ_m are dependent on the base velocity $\dot{x}_b$ considered to be the LPV parameter ρ. Finally, the following qLPV representation of the system is obtained:

$$\dot{\xi} = \begin{bmatrix} 0 & I \\ -\mathcal{M}^{-1}\mathcal{K} & -\mathcal{M}^{-1}\mathcal{C}_m(\rho) \end{bmatrix} \xi + \begin{bmatrix} 0 \\ -\mathcal{M}^{-1}\Lambda \end{bmatrix} w + \begin{bmatrix} 0 \\ \mathcal{M}^{-1}\Gamma_m(\rho) \end{bmatrix} V = A\xi + B_1 w + B_2 V. \tag{5}$$

where A and B_2 matrices are dependent on the scheduling parameter and $w = \ddot{x}_g$ is the ground acceleration considered to be the external disturbance input. It is noted that the base velocity is obtained by low-pass filtering and differentiating the base displacement. In this qLPV model, the system matrices A and B_2 are dependent on the scheduling parameter. Hence, an $\mathcal{H}_\infty$ LPV controller can be designed to reduce the second floor absolute acceleration due to the earthquake excitation by solving an LMI optimization problem [19]. For this purpose, dynamic weights are selected to shape the closed-loop transfer functions. Since we have a regulation problem and tracking is not of concern, we only need to shape the closed-loop transfer functions S and KS in a mixed sensitivity $\mathcal{H}_\infty$ control design formulation [20]. We recall that S is the transfer function between the disturbance $w = \ddot{x}_g$ and the output, and KS is the transfer function between w and the control signal u. The controlled output vector is assumed to be $z = [z_1, z_2]^T = [W_s y, -W_u u]^T$ as shown in Figure 3. The absolute

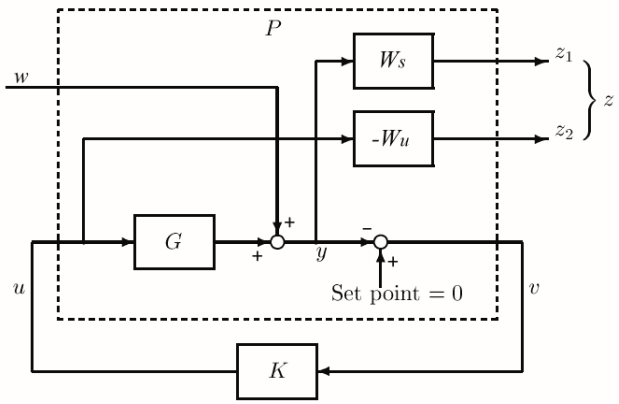

Figure 3. Mixed-sensitivity $\mathcal{H}_\infty$ control design configuration

acceleration of the second floor is considered as the measured output $y = \ddot{x}_2 + \ddot{x}_g$. The dynamic weights for the $\mathcal{H}_\infty$ control design are chosen to be

$$W_u = \frac{2\times 10^{-4} s}{s+20}, \quad W_s = \frac{1.4}{s^2 + 0.9s + 8}.$$

where W_u is the weight on the control input and W_s is the weight on the output. In general, there are two parameter-dependent matrices X and Y in the LMI synthesis conditions corresponding to the LPV $\mathcal{H}_\infty$ control design [21]. One of the Lyapunov matrices Y is set to be linearly dependent on the scheduling parameter, that is, $Y = Y_0 + \rho Y_1$ and the other one is considered to be fixed, *i.e.*, $X = X_0$. The scheduling parameter is chosen to be the damper velocity $\rho = \dot{x}_b$ for which variation and rate bounds are given as follows $\rho \in [-0.3, 0.3]$ m/s and $\dot{\rho} \in [-5, 5]$ m/s^2. The corresponding synthesis LMIs are solved by gridding the parameter space for ρ over its range of variation following the procedure described in [21].

LPV ANTI-WINDUP CONTROL

There are two methods for LPV anti-windup control design in the presence of actuator saturation. One approach in designing the anti-windup compensator involves the design of the original controller in a way to account for actuator nonlinearities. Wu *et al*. [22] employed this method to design an LPV anti-windup controller by using a saturation indicator parameter and used it

to control a linearized aircraft model. This method is beneficial only if a parameter-varying dynamic weight on the control input u is used. The aforementioned method was employed in [23] for control of a mechanical system including an MR damper. A second approach to design anti-windup controllers is based on the traditional two-step approach, where one first designs a controller disregarding the actuator saturation and then adds the anti-windup compensator to accommodate the saturations [24]. In this formulation, the anti-windup controller does not affect the system if saturation is not present. The structure of this method is depicted in Figure 4, in which the arrow indicates the adaptation of the corresponding block with the scheduling parameter.

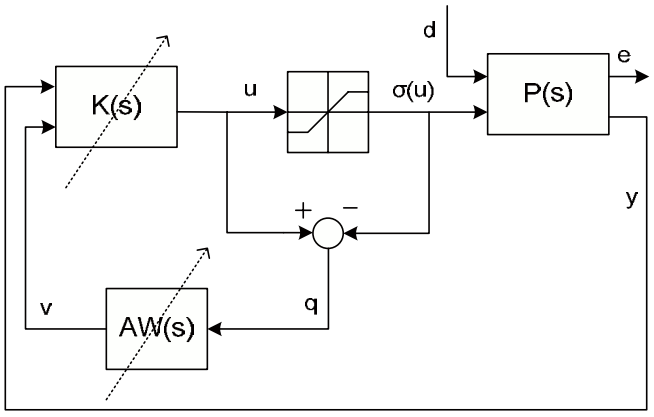

Figure 4. LPV anti-windup control scheme

We consider an LPV system model augmented with the design weights represented by P in Figure 4 that has the following state-space representation:

$$\begin{bmatrix} \dot{x}_p \\ e \\ y \end{bmatrix} = \begin{bmatrix} A_p(\rho) & B_{p1}(\rho) & B_{p2}(\rho) \\ C_{p1}(\rho) & D_{p11}(\rho) & D_{p12}(\rho) \\ C_{p2}(\rho) & D_{p21}(\rho) & D_{p22}(\rho) \end{bmatrix} \begin{bmatrix} x_p \\ d \\ \sigma(u) \end{bmatrix} \tag{6}$$

where $x_p \in R^{n_p}$, $y \in R^{n_y}$, $\sigma(u) \in R^{n_u}$, $e \in R^{n_e}$, and $d \in R^{n_d}$ are the augmented system state, the measurement vector, the saturated control input, the controlled output and the disturbance input, respectively.

The actuator nonlinearities we consider are in the following form

$$\sigma(u_i) = \begin{cases} u_i & |u_i| < u_i^{max} \\ sign(u_i) u_i^{max} & |u_i| \geq u_i^{max} \end{cases} \tag{7}$$

where u_i^{max} is the constant saturation limit for the i-th actuator. To capture the actuator constraints in (7), we define the following

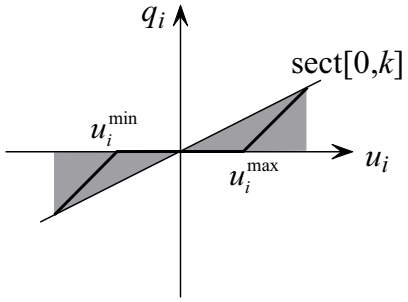

Figure 5. Saturation nonlinearity representation

parameter

$$q_i(u_i) = u_i - \sigma(u_i) \tag{8}$$

which results in the behavior shown in Figure 5, where the slope of the line $\kappa_i \in (0,1)$. Assuming in general n_u control inputs, we define a saturation matrix as $\mathcal{K} = diag(\kappa_1, \kappa_2, ..., \kappa_{n_u})$.

We assume that in (6), $(A_p(\rho), B_{p2}(\rho))$ and $(A_p(\rho), C_{p2}(\rho))$ are parameter-dependent stabilizable and detectable for all ρ, respectively, and that the matrices $[B_{p2}^T(\rho) \quad D_{p12}^T(\rho)]$ and $[C_{p2}(\rho) \quad D_{p21}(\rho)]$ have full row rank, and $D_{p22} = 0$. A nominal LPV controller is designed first by ignoring the actuator saturation using the systematic control design approach in LPV control theory described in [21]. If such a controller exists we pursue with designing an LPV anti-windup compensator such that the adverse effect of input saturations are mitigated in terms of the induced L_2 norm. The dynamic of the anti-windup compensator (depicted by AW in Figure 4) is represented by

$$\begin{bmatrix} \dot{x}_{aw} \\ \upsilon \end{bmatrix} = \begin{bmatrix} A_{aw}(\rho, \dot{\rho}) & B_{aw}(\rho, \dot{\rho}) \\ C_{aw}(\rho, \dot{\rho}) & D_{aw}(\rho, \dot{\rho}) \end{bmatrix} \begin{bmatrix} x_{aw} \\ q \end{bmatrix} \tag{9}$$

The controller K will then be in the following form:

$$\begin{bmatrix} \dot{x}_k \\ u \end{bmatrix} = \begin{bmatrix} A_k(\rho, \dot{\rho}) & B_k(\rho, \dot{\rho}) \\ C_k(\rho, \dot{\rho}) & D_k(\rho, \dot{\rho}) \end{bmatrix} \begin{bmatrix} x_k \\ y \end{bmatrix} + \begin{bmatrix} \upsilon_1 \\ \upsilon_2 \end{bmatrix} \tag{10}$$

where $\upsilon = \begin{bmatrix} \upsilon_1^T & \upsilon_2^T \end{bmatrix}^T$ with $\upsilon_1 \in R^{n_p}$ and $\upsilon_2 \in R^{n_u}$. The system matrices A_k, B_k, C_k, D_k are the state-space representation of the designed unconstrained controller, whereas $A_{aw}, B_{aw}, C_{aw}, D_{aw}$ are the state-space matrices of the anti-windup compensator. The LPV anti-windup control design problem can be then recast into a robust LPV control problem setting where the uncertainties are in the following form:

$$q = \Delta u$$

where $\Delta_i = 1 - \frac{\sigma(u_i)}{u_i}$ and $\Delta = diag(\Delta_1, ..., \Delta_{n_u})$. We use the design method proposed in [24] to design the LPV anti-windup

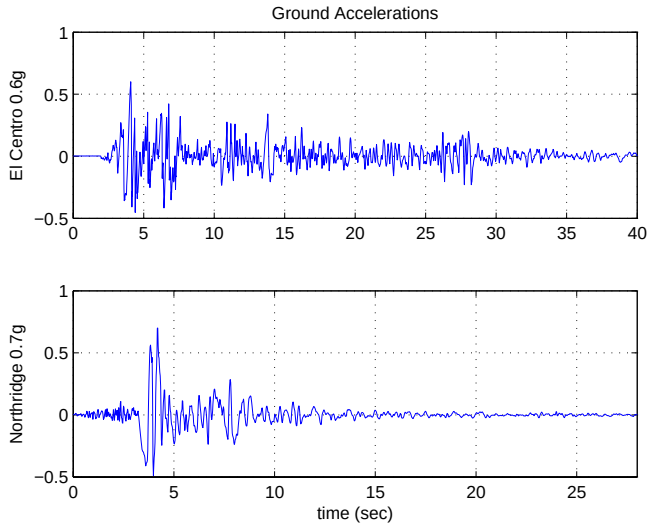

Figure 6. El Centro and Northridge earthquake excitations

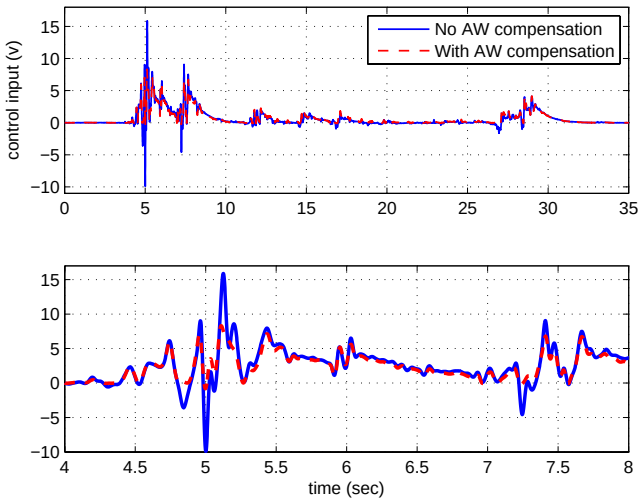

Figure 7. Control input (MR damper voltage) corresponding to El Centro 0.6g- the bottom plot is a zoomed part of the top plot

compensator assuming that the nominal LPV controller K exists. The procedure leading to the anti-windup control design is not repeated here and interested reader is referred to [24] for details.

EXPERIMENTAL RESULTS

Two types of well-known historical earthquake signal forms namely the the El Centro and Northridge are applied as disturbance input to the shaker table described earlier. The intensities of the El Centro and Northridge earthquakes are 0.6g and 0.7g, respectively. Figure 6 shows the two earthquake signals which basically represent the ground acceleration. The following control designs are tested and compared in the MR damper experimental test-bed using the above signals as excitation: (i) an LPV anti-windup controller, (ii) an LPV controller ignoring the actuator saturation phenomena, and (iii) a conventional anti-windup scheme. Due to the space restrictions, we demonstrate the experimental results using only the El Centro test signal.

The LPV anti-windup controller is designed by solving the corresponding LMIs via gridding over the range of base velocity. Gridding is a standard approach to convert infinite-dimensional LMI constraints in the LPV synthesis problem to a set of finite-dimensional LMIs [21]. For simplicity we consider constant basis functions for the Lyapunov functions R_{11}, S, and V in the corresponding synthesis LMIs. The optimal induced $\mathcal{L}_2$-gain is determined to be $\gamma = 6.08$.

First, we compare the cases (i) and (ii), *i.e.*, the designed LPV anti-windup compensator as in Figure 4 with the case with no anti-windup compensation but with a saturation limit of zero and eight volts, for El Centro 0.6g excitation. The control input signal which is the MR damper voltage is depicted in Figure 7 and the second floor acceleration is plotted in Figure 8. The maximum peak of the second floor acceleration for the cases (i) and (ii) is determined to be 4.89 and 4.91 m/s^2, respectively. The

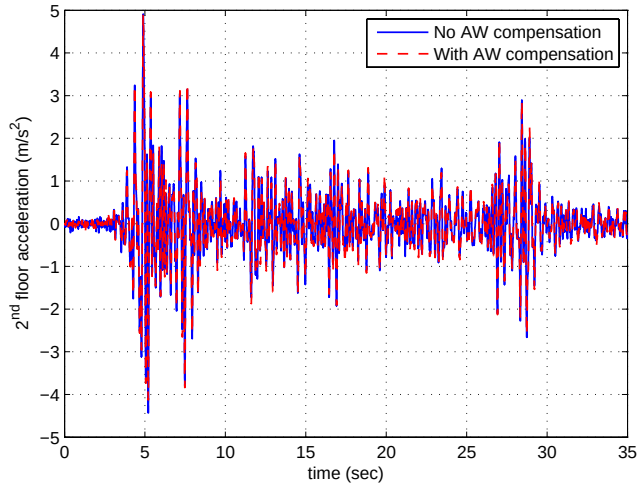

Figure 8. Second floor acceleration corresponding to El Centro 0.6g

root mean square (RMS) for the second floor acceleration for the cases (i) and (ii) is calculated to be 72.72 and 73.38 cm/s^2, respectively. It is observed that the MR damper voltage using the anti-windup compensator is within the allowable range and the performance of the controller is slightly improved. The LPV parameter, based on which the controllers are scheduled is shown in Figure 9.

Next, we compare the results of the designed LPV anti-windup controller (case (i)) with those of a conventional anti-windup scheme (case (iii)). A generic anti-windup scheme is shown in Figure 10, where $G(s)$ and $K(s)$ represent the plant and controller, respectively, while $R(s)$ represents a compensator which feeds back the error between the output from the controller

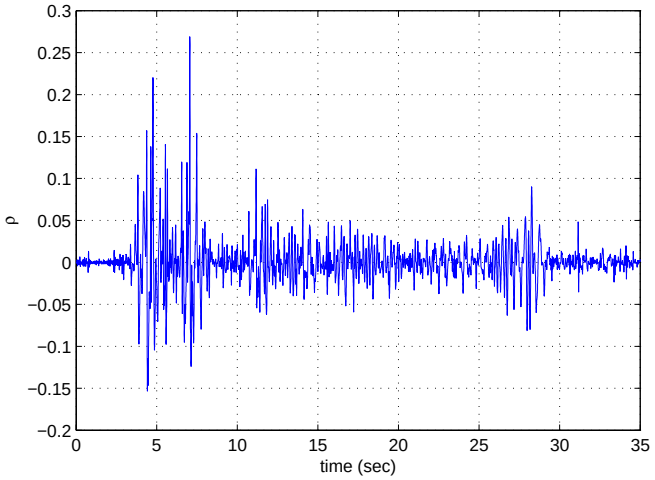

Figure 9. Profile of the scheduling parameter (base velocity in m/s)

and input to the plant. In the classical anti-windup design this compensator is chosen to be $R(s) = \frac{\alpha}{s}$, where the scalar α represents a tunable design parameter [16]. The comparison plots are

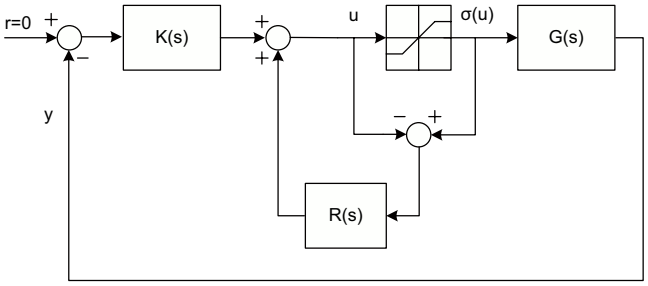

Figure 10. Generic anti-windup scheme

shown in figures 11 and 12. Although the acceleration responses are very similar the voltage input using the LPV anti-windup is meeting the maximum allowable MR damper voltage.

CONCLUSION

In this paper, we designed an LPV anti-windup compensator to complement a nominal LPV controller in order to reduce the vibration of a two-story model structure including an MR damper. Different earthquake signals with different intensities might demand an MR damper voltage out of the tolerable range. By making use of an LPV anti-windup controller the voltage is kept within its allowable limits. The experimental results

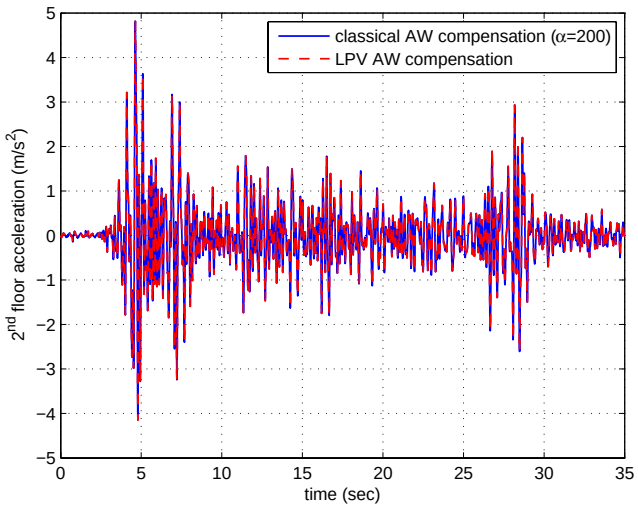

Figure 11. Second floor acceleration corresponding to El Centro 0.6g for a classical AW and an LPV AW design

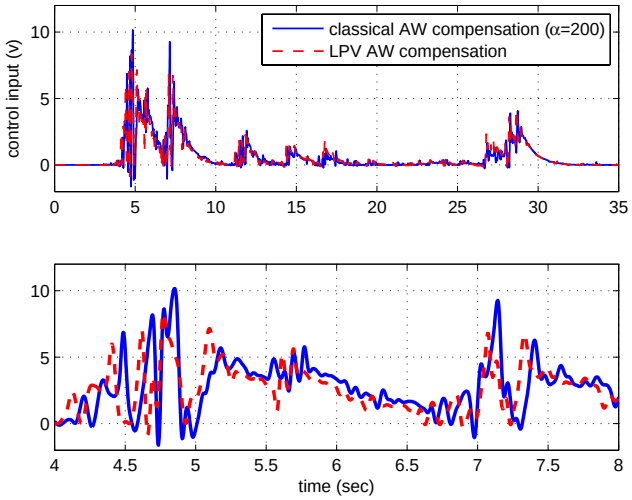

Figure 12. Control input (MR damper voltage) corresponding to El Centro 0.6g- the bottom plot is a zoomed part of the top plot

demonstrate the effectiveness of the employed LPV controller combined with the LPV anti-windup scheme compared to the LPV controller (with no anti-windup compensation), as well as a conventional anti-windup compensation scheme.

REFERENCES

[1] B.F. Spencer, S.J. Dyke, M.K. Sain, and J.D. Carlson, "Phenomenological model of a magnetorheological damper," *Journal of Engineering Mechanics*, 1997.

[2] G. Kamath, N. Wereley and M. Jolly, "Characterization

of magnetorheological helicopter lag dampers," *Journal of Amercian Helicopter Society,* vol. 44, pp. 234-248, 1999.

[3] J. Kim and J. Oh, "Development of an above knee prosthesis using MR damper and leg simulator," *IEEE International Conference on Robatics and Automation*, pp. 3686-3691, 2001.

[4] G. Yao, F. Yap, G. Chen, W. Li, and S. Yeo, "MR damper and its application for semi-active control of vehicle suspension system," *Mechatronics*, vol. 12, pp. 963-973, 2002.

[5] S.J. Dyke, B.F. Spencer Jr., M.K. Sain, and J.D. Carlson, "Modeling of magnetorheological dampers for seismic response reduction," *Smart Materials and Structure*, pp. 565-575, 1996.

[6] C. Sakai, T. Terasawa, and A. Sano, "Integration of bilinear $\mathcal{H}_\infty$ control and adaptive inverse control for semi-active vibration isolation of structures," *in Proc. 44th IEEE Conference on Decision and Control*, 2005.

[7] S. M. Savaresia, S. Bittantia, and M. Montiglio, "Identification of semi-physical and black-box non-linear models: the case of MR-dampers for vehicles control," *Automatica*, vol. 41, pp. 113-127, 2005.

[8] D.L. Guo, H.Y. Hu, and J.Q. Yi, "Neural network control for a semi-active vehicle suspension with a magnetorheological damper," *Journal of Vibration and Control*, vol. 10, no. 3, pp. 461-474, 2004.

[9] L.M. Jansen and S.J. Dyke, "Semi-Active control strategies for MR dampers: A comparative study," *ASCE Journal of Engineering Mechanics*, vol. 126, no. 8, pp. 795-803, 2000.

[10] B. Erkus, M. Abe, and Y. Fujino, "Investigation of semi-active control for seismic protection of elevated highway bridges," *Engineering Structures*, vol. 24, pp. 281-293, 2002.

[11] C. Poussot-Vassal, O. Sename, L. Dugard, P. Gaspar, Z. Szabo, and J. Bokor, "A new semi-active suspension control strategy through LPV technique," *Control Engineering Practice*, vol. 16, pp. 1519-1534, 2008.

[12] H. Du, K.Y. Sze, and J. Lam, "Semi-active $\mathcal{H}_\infty$ control of vehicle suspension with magneto-rheological dampers," *Journal of Sound and Vibration*, vol. 283, pp. 981-996, 2005.

[13] P.J. Campo and M. Morari, "Robust control of processes subject to saturation nonlinearities," *Computers and Chemical Engineering*, vol. 14, pp. 343-358, 1990.

[14] A.R. Teel, "Semi-global stabilization of linear controllable systems with input nonlinearities," *IEEE Trans. on Automatic Control*, vol. 40, pp. 96-100, 1995.

[15] T. Nguyen and F. Jabbari, "Output feedback controllers for disturbance attention with actuator amplitude and rate saturation," *Automatica*, vol. 36, pp. 1339-1346, 2000.

[16] C. Edwards and I. Postlethwaite, "Anti-windup and bumpless transfer schemes," *in Proc. UKACC International Conference on Control*, pp. 394-399, Exeter, UK, 1996.

[17] F. Shirazi, J. Mohammadpour, K. Grigoriadis, and G. Song, "Identification and control of an MR damper with stiction effect and its application in structural vibration mitigation," submitted to *IEEE Trans. on Control System Technology*, Oct. 2010.

[18] W. J. Rugh and J. S. Shamma, "Research on gain scheduling," *Automatica*, 36, pp. 1401-1425, 2000.

[19] P. Gahinet and P. Apkarian, "A linear matrix inequality approach to $\mathcal{H}_\infty$ control," *Int J. Robust and Nonlinear Control*, vol. 4, no. 4, pp. 421-448, 1994.

[20] S. Skogestad and I. Postlethwaite, *Multivariable feedback control analysis and design*, Wiley, 2005.

[21] P. Apkarian and R.J. Adams, "Advanced gain scheduling techniques for uncertain systems," *IEEE Trans. Control Systems Technology*, vol. 6, no. 1, pp. 21-32, 1998.

[22] F. Wu, K.M. Grigoriadis, and A. Packard, "Anti-windup controller design using linear parameter-varying control methods," *International Journal of Control*, vol. 73, no. 12, pp. 1104-1114, 2000.

[23] M. Meisami-Azad, J. Mohammadpour, and K.M. Grigoriadis, "Anti-windup LPV control of magneto-rheological dampers," in Proc. *ASME Dynamic Systems and Control Conference*, Hollywood, CA, Oct. 2009.

[24] B. Lu and F. Wu, "LPV antiwindup compensation for enhanced flight control performance," in Proc. *AIAA Guidance, Navigation, and Control Conference*, Austin, TX, Aug. 2003.